Journal of Vibration Engineering & Technologies (2026) 14:323
https://doi.org/10.1007/s42417-026-02541-5

ORIGINAL PAPER

Robust Vibration Suppression of Double-Pendulum Gantry Cranes via Integral LQR Optimized with an Improved Genetic Algorithm Incorporating Sine–Cosine Operators

Mohamed O. Elhabib[1] · Herman Wahid[1] · Zaharuddin Mohamed[1] · H. I. Jaafar[2] · O. A. Elhabib[3]

Received: 5 February 2026 / Revised: 6 May 2026 / Accepted: 11 May 2026

Abstract

Purpose The control of double-pendulum gantry cranes presents a formidable problem: conflicting objectives of rapid transit and sway suppression contend with underactuated, chaotic dynamics. While the Integral Linear Quadratic Regulator (ILQR) offers a theoretical solution for zero steady-state error, its practical efficacy relies entirely on weighting matrices that standard tuning methods fail to optimize robustly. This study aims to resolve this high-dimensional control problem to ensure stringent industrial safety limits.

Methods An Improved Genetic Algorithm (IGA) is deployed strictly as a supporting optimization tool. By hybridizing the Genetic Algorithm with deterministic Sine Cosine Algorithm (SCA) operators, this approach navigates the complex state-space to uncover optimal vibration control parameters without premature convergence. The system's robustness is systematically evaluated against standard heuristic tunings under both nominal conditions and simultaneous parametric uncertainties (variations in cable length and payload mass).

Results Dynamically, the optimized controller eliminates transient overshoot entirely (0.00%), achieves a rapid settling time of 2.23 s, and minimizes payload residual sway to 4.16°. Statistically, a one-way ANOVA test ($P < 0.001$) and minimal convergence variance (0.0117) validate that the identified parameters represent a robust physical minimum rather than a localized mathematical artifact. Under simultaneous parametric variations, the controller limits worst-case sway to approximately 3.29°, maintaining a superior safety envelope.

Conclusion The IGA-tuned ILQR framework provides a highly robust, empirically validated control architecture. The derived weighting parameters function as practical design guidelines, effectively managing chaotic dynamics and ensuring superior sway-suppression performance regardless of operational parametric uncertainty.

Keywords Gantry crane · Double pendulum crane · Metaheuristic optimization · Genetic Algorithm (GA) · Sine Cosine Algorithm (SCA) · Sway suppression · Optimal control · Robust control

Herman Wahid, Zaharuddin Mohamed, H.I. Jaafar and O.A. Elhabib contributed equally to this work.

✉ Herman Wahid
herman@utm.my

Mohamed O. Elhabib
osman@graduate.utm.my

Zaharuddin Mohamed
zahar@fke.utm.my

H. I. Jaafar
hazriq@utem.edu.my

O. A. Elhabib
osman@tu.edu.sa

[1] Control and Mechatronics Engineering Department, Faculty of Electrical Engineering, Universiti Teknologi Malaysia, Johor Bahru 81310, Malaysia

[2] Faculty of Electrical Engineering, Universiti Teknikal Malaysia Melaka, Melaka, Malaysia

[3] Department of Mechanical Engineering, College of Engineering, Taif University, 21944 Taif, Saudi Arabia

Published online: 29 May 2026

Introduction

Gantry cranes are the backbone of modern heavy industry, serving as the primary logistical nodes in maritime shipping, construction, and large-scale manufacturing [1, 2]. The operational efficiency of these systems is defined by their ability to transport heavy payloads rapidly and precisely. However, this objective presents a formidable control challenge: gantry cranes are underactuated mechanical systems, possessing fewer control inputs (trolley force) than degrees of freedom (trolley position and payload sway). Rapid maneuvers inevitably induce residual oscillations (sway), which not only degrade positioning accuracy but also pose severe safety risks to personnel and infrastructure [1]. Consequently, the development of robust control strategies that can simultaneously ensure fast transient response and effective sway suppression has become a focal point of recent control engineering research [2, 3].

While early research often simplified crane dynamics to a single pendulum model, recent studies have demonstrated that this simplification is insufficient for high-precision applications. In reality, the significant mass of the hoisting hook creates a “double pendulum” effect, where the hook and the payload oscillate at different frequencies [4]. This introduces complex, chaotic, and highly coupled nonlinear dynamics that are sensitive to parameter variations such as cable length and payload mass [4, 5]. Addressing these multi-mode oscillations requires sophisticated control architectures capable of handling high-dimensional state spaces.

To tackle these challenges, various control methodologies have been proposed. Open-loop techniques, such as Input Shaping, have been widely adopted due to their simplicity in vibration reduction. However, their performance is highly sensitive to modeling errors; a slight mismatch in the estimated natural frequency—caused by varying cable lengths—can lead to significant performance degradation [6]. To enhance robustness, closed-loop strategies such as Sliding Mode Control (SMC) and Adaptive Control have been explored [5]. While effective against uncertainties, these nonlinear methods often introduce high structural complexity and the phenomenon of “chattering,” which can cause mechanical wear and actuator saturation. Alternatively, the Linear Quadratic Regulator (LQR) remains a preferred industrial solution [7] due to its mathematically guaranteed stability margins and energy efficiency [8]. The LQR is particularly well-suited for multi-objective problems, as it minimizes a cost function balancing state errors and control effort.

However, the practical efficacy of an LQR controller is entirely dependent on the precise selection of its weighting matrices, Q and R. These matrices determine the trade-off between tracking speed and sway suppression. Traditionally, tuning these parameters is performed via trial-and-error, a process that is not only time-consuming but often fails to locate the optimal solution in the complex, 8-dimensional search space of a double pendulum system [8, 9]. Recent literature has moved towards automating this tuning process using metaheuristic optimization algorithms, such as Genetic Algorithms (GA) [7] and Particle Swarm Optimization (PSO) [10]. While these methods outperform manual tuning, standard metaheuristics suffer from a critical limitation known as “premature convergence” [11]. As noted in recent comparative reviews [12, 13], standard GAs often lose population diversity early in the search process, becoming trapped in local optima. This results in “brittle” controllers that perform well at a nominal operating point but fail when the crane’s payload mass or cable length varies.

To bridge this gap, this paper proposes a novel Improved Genetic Algorithm (IGA) for the robust tuning of an Integral-LQR (ILQR) controller. The IGA addresses the premature convergence of standard GA by hybridizing it with the deterministic search mechanisms of the Sine Cosine Algorithm (SCA). Recent studies in feature selection [14] and mathematical optimization [15] have proven that the mathematical fluctuation of sine and cosine functions facilitates a better balance between exploration (searching the global space) and exploitation (refining local solutions). By integrating SCA operators [14] with adaptive crossover and mutation probabilities [16–18], the proposed IGA dynamically maintains population diversity, preventing stagnation in local optima [19]. This approach allows the algorithm to navigate the complex constraints of the double pendulum system more effectively than standard evolutionary methods [20–22].

This work establishes explicit, transferable design guidance for weighting LQR states in double-pendulum systems. Characterizing the stability and robustness envelopes of the crane across extensive parameter sweeps reveals the physical limitations and optimal balancing of multi-mode sway dynamics. The derived physical limits and robust performance envelopes hold independently of the specific optimization architecture used to locate them. This approach establishes a highly practical framework for high-precision industrial crane automation.

The remainder of this paper is organized as follows. Section “System Modeling and Preliminaries” details the complete nonlinear dynamic modeling of the double-pendulum gantry crane and its subsequent linearization. Section “Proposed Control Strategy: IGA-Tuned ILQR” presents the proposed ILQR control architecture and formulates the parameter selection process, introducing the IGA strictly as a supporting optimization tool utilized to derive the necessary weighting matrices. Section “Simulation Results Analysis” provides a comprehensive simulation analysis, evaluating the sway-suppression performance and robust control behavior of the proposed system against standard heuristically tuned controllers in both nominal and parametric disturbance scenarios. Finally, Section "Discussion" discusses the empirically derived physical design insights, and Section "Conclusions presents the conclusions.

System Modeling and Preliminaries

Dynamic Model Derivation

This section details the derivation of the dynamic model for the Double-Pendulum Gantry Crane under the condition of a fixed cable length. The physical representation of the system is illustrated in Fig. 1. The model is characterized by three independent generalized coordinates: the horizontal position of the trolley, denoted by x; the swing angle of the hook θ_1; and the swing angle of the payload θ_2. The physical parameters of the system are defined as follows: M is the trolley mass, m_1 is the hook mass, and m_2 is the payload mass. The fixed cable length between the trolley and the hook is l_1, while the length of the sling cable between the hook and the payload is l_2. The model also considers the input force $u = F_x$ applied to the trolley, the viscous damping coefficient of the trolley f_x, and the gravitational acceleration constant g [23].

The dynamic equations of motion are systematically derived using the Euler-Lagrange method, which is a powerful technique for analyzing complex mechanical systems. The general form of the Lagrange equation is given by:

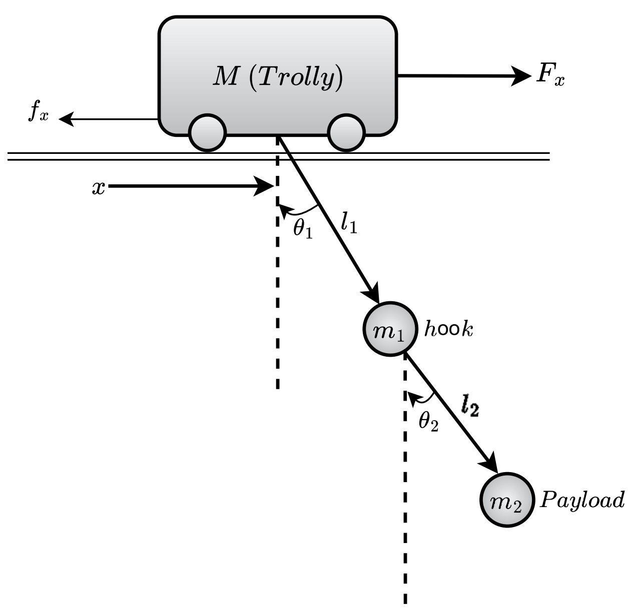

Fig. 1 Schematic diagram of the double-pendulum gantry crane system illustrating the generalized coordinates (x, θ_1, θ_2), system masses (M, m_1, m_2), and acting forces

$$\frac{d}{dt}\left(\frac{\partial L}{\partial \dot{q}_i}\right) - \frac{\partial L}{\partial q_i} = T_i \tag{1}$$

where L is the Lagrangian function, q_i represents the generalized coordinates $\mathrm{q} = [x, \theta_1, \theta_2]^T$, and T_i is the non-conservative generalized force. The Lagrangian L is defined as the difference between the total kinetic energy K and the total potential energy P of the system.

$$L = K - P \tag{2}$$

Kinetic Energy Derivation

The total kinetic energy K of the system is the summation of the kinetic energies of the trolley (K_x), the hook (K_{θ_1}), and the payload (K_{θ_2}).

$$K = K_x + K_{\theta_1} + K_{\theta_2} \tag{3}$$

The individual kinetic energy components are defined as:

$$K_x = \frac{1}{2}M\dot{x}^2 \tag{4}$$

$$K_{\theta_1} = \frac{1}{2}m_1 v_1^2 \tag{5}$$

$$K_{\theta_2} = \frac{1}{2}m_2 v_2^2 \tag{6}$$

Here, $\dot{x}$ is the trolley velocity, while v_1 and v_2 are the velocity vectors of the hook and payload, respectively. The squared magnitudes of these velocities are derived from their Cartesian components:

$$v_1^2 = (\dot{x} + l_1\dot{\theta}_1\cos\theta_1)^2 + (l_1\dot{\theta}_1\sin\theta_1)^2 \tag{7}$$

$$v_2^2 = (\dot{x} + l_1\dot{\theta}_1\cos\theta_1 + l_2\dot{\theta}_2\cos\theta_2)^2 + (l_1\dot{\theta}_1\sin\theta_1 + l_2\dot{\theta}_2\sin\theta_2)^2 \tag{8}$$

By substituting these expressions into Eq. 3, the complete kinetic energy K of the system is formulated as:

$$\begin{aligned} K = {} & \frac{1}{2}M\dot{x}^2 + \frac{1}{2}m_1(\dot{x}^2 + 2\dot{x}l_1\dot{\theta}_1\cos\theta_1 + l_1^2\dot{\theta}_1^2) \\ & + \frac{1}{2}m_2(\dot{x}^2 + 2\dot{x}l_1\dot{\theta}_1\cos\theta_1 + 2\dot{x}l_2\dot{\theta}_2\cos\theta_2 \\ & + l_1^2\dot{\theta}_1^2 + l_2^2\dot{\theta}_2^2 + 2l_1l_2\dot{\theta}_1\dot{\theta}_2\cos(\theta_1 - \theta_2)) \end{aligned} \tag{9}$$

Potential Energy Derivation

The total potential energy P is determined by the gravitational potential energy of the hook (P_{θ_1}) and the payload

(P_{θ_2}). The potential energy of the trolley is considered to be zero as its vertical position remains constant ($P_x = 0$).

$$P = P_{\theta_1} + P_{\theta_2} \tag{10}$$

The individual potential energies are functions of their vertical displacements, h_1 and h_2:

$$P_{\theta_1} = m_1 g h_1 \tag{11}$$

$$P_{\theta_2} = m_2 g(h_1 + h_2) \tag{12}$$

The vertical displacements are given by $h_1 = l_1(1 - \cos\theta_1)$ and $h_2 = l_2(1 - \cos\theta_2)$. Therefore, the complete potential energy P of the system is:

$$P = m_1 g l_1(1 - \cos\theta_1) + m_2 g(l_1(1 - \cos\theta_1) + l_2(1 - \cos\theta_2)) \tag{13}$$

Lagrangian and Equations of Motion

By applying the Euler-Lagrange Eq. 1 to the Lagrangian L with respect to each generalized coordinate yields the nonlinear dynamic model of the system. For clarity and subsequent control design, the resulting set of three coupled, highly nonlinear differential equations is expressed in the standard matrix form for mechanical systems:

$$\mathrm{M}(q)\ddot{q} + \mathrm{C}(q,\dot{q})\dot{q} + \mathrm{G}(q) = \mathrm{F} \tag{14}$$

where $\mathrm{q} = [x, \theta_1, \theta_2]^T$ is the vector of generalized coordinates. The components of this equation, namely the symmetric positive-definite mass matrix $\mathrm{M}(q)$, the vector of Coriolis and centrifugal forces $\mathrm{C}(q,\dot{q})\dot{q}$ (which also includes viscous damping effects), the gravitational vector $\mathrm{G}(q)$, and the vector of generalized external forces F, are defined where, for conciseness, the trigonometric notations $c_i = \cos(\theta_i)$, $s_i = \sin(\theta_i)$, $c_{12} = \cos(\theta_1 - \theta_2)$, and $s_{12} = \sin(\theta_1 - \theta_2)$ have been used.

The **Mass Matrix** $\mathrm{M}(q)$ is given by:

$$\mathrm{M}(q) = \begin{bmatrix} M + m_1 + m_2 & (m_1 + m_2)l_1 c_1 & m_2 l_2 c_2 \\ (m_1 + m_2)l_1 c_1 & (m_1 + m_2)l_1^2 & m_2 l_1 l_2 c_{12} \\ m_2 l_2 c_2 & m_2 l_1 l_2 c_{12} & m_2 l_2^2 \end{bmatrix} \tag{15}$$

The Coriolis, Centrifugal, and Damping Vector $\mathrm{C}(q,\dot{q})\dot{q}$ is:

$$\mathrm{C}(q,\dot{q})\dot{q} = \begin{bmatrix} f_x\dot{x} - (m_1 + m_2)l_1\dot{\theta}_1^2 s_1 - m_2 l_2\dot{\theta}_2^2 s_2 \\ m_2 l_1 l_2 \dot{\theta}_2^2 s_{12} \\ -m_2 l_1 l_2 \dot{\theta}_1^2 s_{12} \end{bmatrix} \tag{16}$$

The Gravitational Vector $\mathrm{G}(q)$ is:

$$\mathrm{G}(q) = \begin{bmatrix} 0 \\ (m_1 + m_2) g l_1 s_1 \\ m_2 g l_2 s_2 \end{bmatrix} \tag{17}$$

The Generalized Force Vector F is:

$$\mathrm{F} = \begin{bmatrix} F_x \\ 0 \\ 0 \end{bmatrix} \tag{18}$$

State-Space Representation and Linearization

For the purpose of designing a linear controller, such as the LQR, the highly non-linear dynamic model derived in the previous section must be linearized around a stable operating point. The standard state-space representation provides a convenient and powerful framework for this analysis. First, we define a state vector $\mathrm{X} \in \mathbb{R}^6$ that comprehensively describes the system's dynamic state. The vector is chosen to include the generalized positions and their corresponding velocities:

$$\mathrm{X} = [x, \theta_1, \theta_2, \dot{x}, \dot{\theta}_1, \dot{\theta}_2]^T = [q^T, \dot{q}^T]^T \tag{19}$$

Using this state vector, the nonlinear matrix Eq. 14 can be expressed in the general nonlinear state-space form $\dot{\mathrm{X}} = f(\mathrm{X}, u)$, where the input $u = F_x$.

The system is linearized around the natural equilibrium point, where the trolley is at rest and the pendulums are hanging vertically without motion. This corresponds to the origin of the state-space, where $\mathrm{X}_{eq} = 0$ and the input is $u_{eq} = 0$. The linearization is performed using the first-order Taylor series expansion of the non-linear dynamics, resulting in the well-known linear time-invariant (LTI) state-space model:

$$\dot{\mathrm{X}} = \mathrm{AX} + \mathrm{B}u \tag{20}$$

$$\mathrm{y} = \mathrm{CX} + \mathrm{D}u \tag{21}$$

The system matrix A and the input matrix B are the Jacobians of the non-linear system dynamics evaluated at the equilibrium point: $\mathrm{A} = \left.\frac{\partial f}{\partial \mathrm{X}}\right|_{\mathrm{X}_{eq}, u_{eq}}$ and $\mathrm{B} = \left.\frac{\partial f}{\partial u}\right|_{\mathrm{X}_{eq}, u_{eq}}$.

For the Double Pendulum Gantry Crane system, these matrices take the following block structure:

$$\mathrm{A} = \begin{bmatrix} 0_{3\times3} & \mathrm{I}_{3\times3} \\ -\mathrm{M}_{eq}^{-1}\mathrm{K}_g & -\mathrm{M}_{eq}^{-1}\mathrm{D}_{eq} \end{bmatrix} \tag{22}$$

$$\mathrm{B} = \begin{bmatrix} 0_{3\times1} \\ \mathrm{M}_{eq}^{-1}\begin{bmatrix} 1 \\ 0 \\ 0 \end{bmatrix} \end{bmatrix} \tag{23}$$

where 0 and I are the zero and identity matrices of appropriate dimensions, respectively. The matrices M_{eq}, D_{eq}, and K_g are the constant mass, damping, and stiffness matrices evaluated at the equilibrium point (i.e., $\cos(\theta_i) \to 1$, $\sin(\theta_i) \to \theta_i$).

The control objective is to regulate the cart position and pendulum angles. Therefore, the output vector is chosen as $\mathrm{y} = [x, \theta_1, \theta_2]^T$. The corresponding output matrix C and feedthrough matrix D are:

$$\mathrm{C} = [\mathrm{I}_{3\times 3} \quad 0_{3\times 3}], \quad \mathrm{D} = 0_{3\times 1} \tag{24}$$

The specific component matrices required to construct the state-space model are derived by evaluating the mass matrix $\mathrm{M}(q)$, damping terms, and gravitational terms at the equilibrium point ($q = 0, \dot{q} = 0$).

The constant, symmetric Mass Matrix at Equilibrium, M_{eq}, is found by setting all angles to zero in Eq. 15:

$$\mathrm{M}_{eq} = \begin{bmatrix} M + m_1 + m_2 & (m_1 + m_2)l_1 & m_2 l_2 \\ (m_1 + m_2)l_1 & (m_1 + m_2)l_1^2 & m_2 l_1 l_2 \\ m_2 l_2 & m_2 l_1 l_2 & m_2 l_2^2 \end{bmatrix} \tag{25}$$

The linearized Stiffness Matrix, K_g, results from the gravitational vector $\mathrm{G}(q)$ by assuming $\sin(\theta_i) \approx \theta_i$:

$$\mathrm{K}_g = \begin{bmatrix} 0 & 0 & 0 \\ 0 & (m_1 + m_2) g l_1 & 0 \\ 0 & 0 & m_2 g l_2 \end{bmatrix} \tag{26}$$

The linearized Damping Matrix, D_{eq}, includes only the viscous friction of the trolley, as pivot damping is considered negligible in this model:

$$\mathbf{D_{eq}} = \begin{bmatrix} f_x & 0 & 0 \\ 0 & 0 & 0 \\ 0 & 0 & 0 \end{bmatrix} \tag{27}$$

These matrices are then used to populate the system matrix A as defined in Eq. 22. The resulting state-space model accurately represents the system's local dynamics for small deviations around the equilibrium and forms the basis for the linear controller design.

Problem Formulation

The fundamental challenge in Double Pendulum Gantry Crane is to design a control law for the horizontal force applied to the trolley, $u(t) = F_x$, that steers the system from an initial state of rest to a desired final state. The scope of this work is confined to maneuvers with fixed cable lengths meaning no hoisting or lowering of the payload occurs during transport. This maneuver must be executed while simultaneously satisfying two primary, and often conflicting, performance objectives.

Let the state of the system be described by the vector of generalized coordinates $\mathbf{q(t)} = [x(t), \theta_1(t), \theta_2(t)]^T$. The control objectives are formulated as follows:

1. **Position Tracking:** The trolley's position, $x(t)$, must precisely and rapidly follow a given reference trajectory $x_r(t)$. This requires that the tracking error, defined as $e(t) = x_r(t) - x(t)$, asymptotically converges to zero. Mathematically, this is expressed as:

$$\lim_{t\to\infty} |x_r(t) - x(t)| = 0 \tag{28}$$

   This objective must be met with desirable transient performance, including minimal overshoot and a fast settling time.

2. **Sway Suppression:** During the transportation phase and upon its completion, the sway angles of both the hook ($\theta_1(t)$) and the payload ($\theta_2(t)$) must be effectively suppressed. Any induced oscillations must be rapidly damped, ensuring the payload remains stationary at the final configuration. This objective is formally stated as:

$$\lim_{t\to\infty} \theta_1(t) = 0 \quad \text{and} \quad \lim_{t\to\infty} \theta_2(t) = 0 \tag{29}$$

Achieving these objectives concurrently is non-trivial due to the inherent dynamic coupling and the underactuated nature of the system, wherein a single control input must manage three distinct degrees of freedom. The control law must therefore be designed to find an optimal balance between trolley positioning and the effective attenuation of crane swing dynamics

Proposed Control Strategy: IGA-Tuned ILQR

Control Law Development

The standard Linear-Quadratic Regulator (LQR) is an optimal state feedback controller designed for regulation problems, where the objective is to drive the system states to the origin [24]. However, for the reference tracking task formulated previously, the standard LQR does not inherently possess the structure required to guarantee zero steady-state error. In the presence of modeling inaccuracies or unmodeled, constant external disturbances, a conventional LQR controller will typically exhibit a non-zero steady-state tracking error. To address this fundamental limitation and ensure robust asymptotic tracking, the controller architecture is augmented with integral action. This is achieved by incorporating the integral of the tracking error into the state vector, a technique that systematically enforces Type 1 servo-mechanism behavior, thereby ensuring zero steady-state error for step-like references and disturbances.

To implement the integral control action, we first define the tracking error for the trolley's position as $e(t) = x_r(t) - x(t)$, where $x_r(t)$ is the desired reference trajectory. An integral state variable, $\xi(t)$, is then introduced, whose dynamic is governed by the tracking error:

$$\dot{\xi}(t) = e(t) = x_r(t) - x(t) \tag{30}$$

The original state vector $\mathrm{X}(t) \in \mathbb{R}^6$ is now augmented with this integral state to form a new augmented state vector $\mathrm{X}_{aug}(t) \in \mathbb{R}^7$:

$$\mathrm{X}_{aug}(t) = \begin{bmatrix} \mathrm{X}(t) \\ \xi(t) \end{bmatrix} \tag{31}$$

The dynamics of this augmented state vector can be derived from the linearized system model in Eq. 20 and the definition of the integral state. The trolley position $x(t)$ corresponds to the first element of the state vector $\mathrm{X}(t)$, allowing us to write $x(t) = \mathrm{C}_x\mathrm{X}(t)$ where $\mathrm{C}_x = [1 \quad 0 \quad \cdots \quad 0]$. Consequently, the augmented state-space model can be expressed as:

$$\dot{\mathrm{X}}_{aug} = \mathrm{A}_{aug}\mathrm{X}_{aug} + \mathrm{B}_{aug}u + \mathrm{E}_{aug}x_r \tag{32}$$

where the augmented system matrices $\mathrm{A}_{aug} \in \mathbb{R}^{7\times 7}$, $\mathrm{B}_{aug} \in \mathbb{R}^{7\times 1}$, and the reference input matrix $\mathrm{E}_{aug} \in \mathbb{R}^{7\times 1}$ are constructed in block-matrix form as follows:

$$\mathrm{A}_{aug} = \begin{bmatrix} \mathrm{A} & 0_{6\times 1} \\ -\mathrm{C}_x & 0 \end{bmatrix}, \quad \mathrm{B}_{aug} = \begin{bmatrix} \mathrm{B} \\ 0 \end{bmatrix}, \quad \mathrm{E}_{aug} = \begin{bmatrix} 0_{6\times 1} \\ 1 \end{bmatrix} \tag{33}$$

The ILQR control problem is to find an optimal control law $u(t)$ as in Fig. 2, which minimizes a quadratic performance index J, defined over an infinite time horizon. This cost function penalizes deviations in the augmented state and the magnitude of the control effort:

$$J = \int_0^\infty (\mathrm{X}_{aug}^T(t)\mathrm{Q}_{aug}\mathrm{X}_{aug}(t) + u^T(t)\mathrm{R}u(t))dt \tag{34}$$

Here, $\mathrm{Q}_{aug} \in \mathbb{R}^{7\times 7}$ is the semi-positive definite state weighting matrix ($\mathrm{Q}_{aug} \geq 0$), and $\mathrm{R} \in \mathbb{R}^{1\times 1}$ is the positive definite control weighting matrix ($\mathrm{R} > 0$) [25]. The selection of these weighting matrices is critical, as it dictates the trade-off between tracking performance, sway suppression, and control energy consumption.

The solution to this linear-quadratic optimization problem is a full-state feedback control law that is linear in the augmented state vector, assuming the reference x_r is handled by the integrator and is zero for the regulation problem itself:

$$u(t) = -\mathrm{K}_{aug}\mathrm{X}_{aug}(t) \tag{35}$$

The optimal gain matrix, $\mathrm{K}_{aug} \in \mathbb{R}^{1\times 7}$, is calculated from the unique, symmetric, positive definite solution P to the

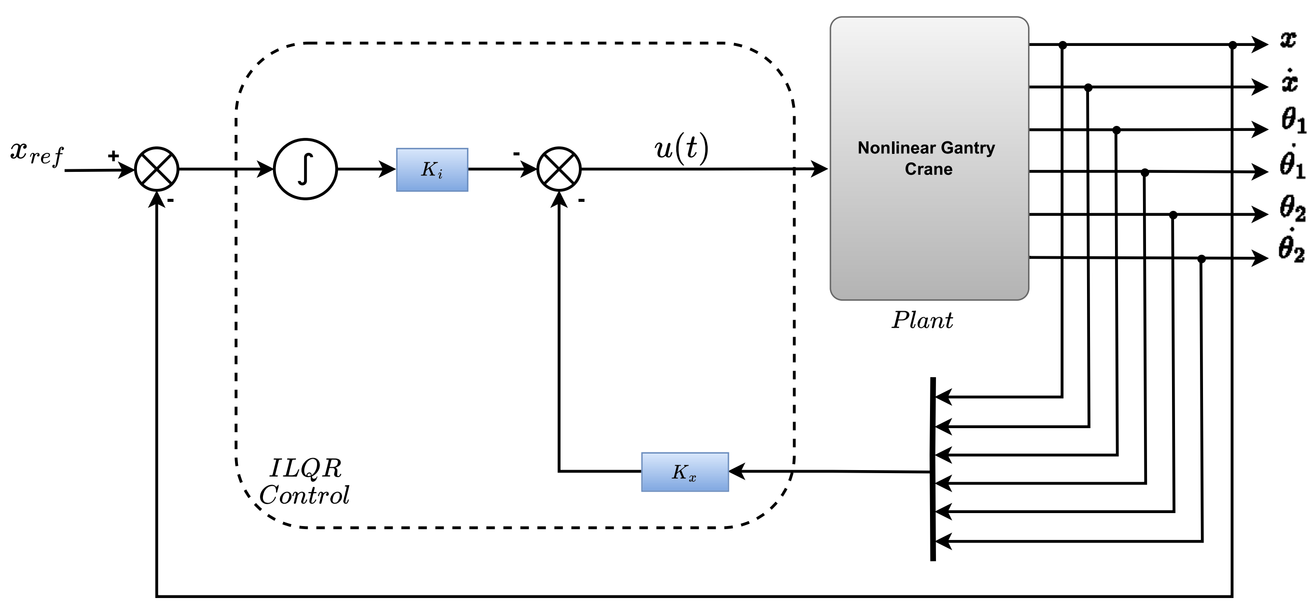

Fig. 2 ILQR configuration with gantry crane system

continuous-time Algebraic Riccati Equation (ARE) for the augmented system:

$$\mathrm{A}_{aug}^T\mathrm{P} + \mathrm{P}\mathrm{A}_{aug} - \mathrm{P}\mathrm{B}_{aug}\mathrm{R}^{-1}\mathrm{B}_{aug}^T\mathrm{P} + \mathrm{Q}_{aug} = 0 \tag{36}$$

Given the solution P, the optimal feedback gain matrix is computed as:

$$\mathrm{K}_{aug} = \mathrm{R}^{-1}\mathrm{B}_{aug}^T\mathrm{P} \tag{37}$$

This control law guarantees closed-loop stability and optimality with respect to the cost function *J*, provided the pair $(\mathrm{A}_{aug}, \mathrm{B}_{aug})$ is stabilizable and the pair $(\mathrm{Q}_{aug}^{1/2}, \mathrm{A}_{aug})$ is detectable.

For implementation, the optimal gain matrix K_{aug} is conceptually partitioned to correspond with the original state vector $\mathrm{X}(t)$ and the appended integral state $\xi(t)$. This partitioning yields a state feedback gain matrix $\mathrm{K}_X \in \mathbb{R}^{1\times 6}$ and a scalar integral gain K_ξ:

$$\mathrm{K}_{aug} = [\mathrm{K}_X \quad K_\xi] \tag{38}$$

Substituting this partitioned gain into the control law from Eq. 35 provides the explicit structure of the controller:

$$u(t) = -\mathrm{K}_{aug}\mathrm{X}_{aug}(t) = -(\mathrm{K}_X\mathrm{X}(t) + K_\xi\xi(t)) \tag{39}$$

By substituting the integral definition of $\xi(t)$ from Eq. 30, the final implementable form of the ILQR control law is obtained:

$$u(t) = -\mathrm{K}_X\mathrm{X}(t) - K_\xi \int_0^t (x_r(\tau) - x(\tau))d\tau \tag{40}$$

The control signal is thus composed of two distinct components. The first term, $-\mathrm{K}_X\mathrm{X}(t)$, constitutes the proportional state feedback action, which is responsible for stabilizing the closed-loop system and shaping its transient dynamics. The second term, $-K_\xi \int_0^t e(\tau)d\tau$, represents the integral action that actively works to eliminate any persistent tracking error, thereby ensuring robust asymptotic reference tracking. The fundamental challenge in this design, which is the subject of the subsequent section, is the optimal selection of the weighting matrices Q_{aug} and R that produce the gain matrix K_{aug}.

Formulation of the Optimization Problem

The performance of the ILQR controller derived in the previous section is critically dependent on the selection of the weighting matrices, Q_{aug} and R. Manual tuning of these matrices is a heuristic, time-consuming process that rarely yields a truly optimal solution, especially for a multi-objective problem involving both tracking and sway suppression. To overcome this limitation, a systematic optimization approach is formulated to automatically find the weighting parameters that result in the best possible system performance.

To simplify the optimization problem and reduce the dimensionality of the search space, the decision variables are the weighting matrices and constrained to be diagonal. The state weighting matrix Q_{aug} is a 7×7 diagonal matrix, and the control weighting matrix R is a positive scalar, as there is a single control input. The set of parameters to be optimized, known as the decision variables, is consolidated into a single vector $\mathrm{z} \in \mathbb{R}^8$:

$$\mathrm{z} = [q_1 \quad q_2 \quad q_3 \quad q_4 \quad q_5 \quad q_6 \quad q_7 \quad r]^T \tag{41}$$

where $q_1, \ldots, q_7$ are the diagonal elements of Q_{aug} corresponding to the states of the system and *r* is the scalar value of R.

The control framework addresses the dichotomous objectives of minimizing trolley tracking error (e_x) and damping pendular sway angles (θ_1, θ_2). Accordingly, the Integral of Absolute Error (IAE) is adopted to quantify global system performance. To mitigate the issue of dimensional commensurability between translational (meters) and rotational (radians) variables, a normalized objective formulation is implemented. This normalization strategy inherently balances the state penalties without requiring arbitrary external weighting factors (w_i). The scalar objective function J_{opt} is thus defined as:

$$J_{opt}(\mathrm{z}) = \int_0^{t_f} \left(\frac{|x_{ref}(t) - x(t)|}{x_{max}} + \frac{|\theta_1(t)|}{\theta_{1,max}} + \frac{|\theta_2(t)|}{\theta_{2,max}} \right) dt \tag{42}$$

where the normalization bounds are defined by the operational safety constraints: the maximum target trolley displacement $x_{max} = 0.4$ m and the maximum permissible sway angles $\theta_{1,max} = \theta_{2,max} = 10^\circ$ (≈ 0.1745 rad). By scaling the error terms against these specific physical limits, the optimization algorithm is driven to minimize the relative violation of safety constraints rather than being biased by the numerical magnitude differences between position and angle states.

The optimization framework is formulated to identify the optimal decision vector z that minimizes the objective function J_{opt}, subject to strict parametric constraints. The formal problem definition is given by:

$$\min_{\mathrm{z}} J_{opt}(\mathrm{z}) \tag{43}$$

subject to the box constraints:

$$z_{lb} \leq z \leq z_{ub} \tag{44}$$

where the boundary vectors z_{lb} and z_{ub} are defined as:

$$\begin{aligned} z_{lb} &= [0 \quad 0 \quad 0 \quad 0 \quad 0 \quad 0 \quad 0 \quad 0.0001]^T \\ z_{ub} &= [300 \quad 100 \quad 100 \quad 20 \quad 100 \quad 20 \quad 2000 \quad 1]^T \end{aligned} \tag{45}$$

The delineation of this search space is governed by two critical physical and theoretical prerequisites. First, the decision variable bounds are calibrated to ensure the resulting feedback gains produce a control effort compliant with the actuator's operational capacity, strictly confining the force within the saturation limits of $-1\ \mathrm{N} \leq u(t) \leq 1\ \mathrm{N}$. Second, the lower bounds enforce the necessary conditions for closed-loop stability; specifically, they guarantee that the state weighting matrix Q remains positive semi-definite and the control weighting scalar R remains positive definite. Adherence to these conditions ensures the solvability of the Algebraic Riccati Equation (ARE), thereby guaranteeing the asymptotic stability of the optimized control system.

Improved GA Based ILQR Controller Optimization

The efficacy of the ILQR control law is fundamentally determined by the choice of its weighting matrices, Q_{aug} and R . To replace heuristic manual tuning with a systematic and robust optimization procedure, this work proposes a novel Adaptive Genetic Algorithm (AGA). The core innovation lies in replacing the canonical probabilistic genetic operators with dynamic operators guided by the mathematical framework of the Sine Cosine Algorithm (SCA) [26]. This creates a parameter-light algorithm that naturally transitions from a global, exploratory search phase to a local, exploitative fine-tuning phase.

IGA Components and Workflow

The optimization process operates on a population of candidate solutions, where each individual (or chromosome) represents a complete set of ILQR tuning parameters. The algorithm evolves this population over successive generations to find the optimal parameter set that minimizes the performance objective function.

1. **Chromosome Representation and Fitness Evaluation:** Each chromosome in the population is encoded as the decision vector $z \in \mathbb{R}^8$, as defined in Eq. 41. The fitness of a chromosome is the inverse of its objective function score, $Fitness = J_{opt}(z)$, where J_{opt} is the IAE-based performance index from Eq. 42. The evaluation of a single chromosome's fitness is a multi-step process:
   - The chromosome vector z is decoded to construct the diagonal weighting matrices Q_{aug} and R.
   - These matrices are used to solve the Algebraic Riccati Eq. 36 for the unique positive definite solution P.
   - The ILQR gain matrix K_{aug} is computed using Eq. 37.
   - A full simulation of the system is performed using the control law $u(t) = -K_{aug}X_{aug}(t)$.
   - The objective function J_{opt} is calculated from the simulation results, and the fitness is determined.

2. **Selection Mechanism:** A tournament selection strategy is employed to choose parent individuals for breeding. In this method, a small subset of individuals is randomly selected from the population, and the individual with the best fitness within that subset is chosen as a parent. This process is repeated to select the required number of parents for the next generation.
3. **Adaptive Genetic Operators:** The core of the proposed IGA lies in its novel crossover and mutation operators, which are applied deterministically in every generation. Their behavior is governed by a master control parameter, r_1, which decays linearly from a constant *a* to 0 over the total number of generations, T_{max}:

$$r_1 = a - t\frac{a}{T_{max}} \tag{46}$$

   where *t* is the current generation number.

   - **Sine Cosine Crossover (SCX):** Given two parent chromosomes, P_1 and P_2, the SCX operator generates two offspring, O_1 and O_2, using the following equations:

$$O_1 = P_1 + r_1 \sin(r_2)|P_2 - P_1| \tag{47}$$

$$O_2 = P_2 + r_1 \cos(r_2)|P_1 - P_2| \tag{48}$$

   where $r_2 \in [0, 2\pi]$ is a random number updated for each operation. In early generations ($r_1 > 1$), this operator promotes exploration by creating offspring potentially far from the parents. In later generations ($r_1 < 1$), it promotes exploitation by generating offspring between the parents.

   - **SCA-Guided Mutation (SCM):** The SCM operator modifies an individual chromosome X_i by guiding it toward the current global best solution, P_{best}, with a dynamically adjusted step size:

$$X_i' = X_i + r_1 \left(\frac{\sin(r_2) + \cos(r_2)}{2} \right) |P_{best} - X_i| \tag{49}$$

The mutation strength is directly proportional to r_1, providing strong exploratory mutations early in the search and weak, fine-tuning mutations as the search converges.

IGA Algorithm Pseudocode

The complete optimization procedure, which integrates the ILQR design within the IGA framework and incorporates elitism to preserve the best solution found, is detailed in Algorithm 1.

Algorithm 1 IGA-Based ILQR Optimization.

Input: Population size N, max generations T_{max}, bounds $[\mathbf{z}_{lb}, \mathbf{z}_{ub}]$, SCA parameter a
Output: Optimal ILQR decision vector $\mathbf{z}_{best}$
▷ Initialization Phase
Initialize population $\mathbf{Z} \leftarrow \{\mathbf{z}_1, \dots, \mathbf{z}_N\}$, where $\mathbf{z}_i \sim \mathcal{U}(\mathbf{z}_{lb}, \mathbf{z}_{ub})$
for $\forall \mathbf{z}_i \in \mathbf{Z}$ **do**
  Extract $\mathbf{Q}_{aug}$, $\mathbf{R}$ from $\mathbf{z}_i$; Solve ARE Eq. 36 for $\mathbf{P}$
  $J_i \leftarrow J_{opt}(\mathbf{z}_i)$ via Eq. 42 **if** $\mathbf{P} \succ 0$, **else** $J_i \leftarrow \infty$
end for
$\mathbf{z}_{best} \leftarrow \arg\min_{\mathbf{z}_i \in \mathbf{Z}} J_i$; $J_{best} \leftarrow \min(J_i)$
▷ Evolutionary Main Loop
for $t = 1$ to T_{max} **do**
  $r_1 \leftarrow a - t(a/T_{max})$ ▷ Update master control parameter
  $\mathbf{Z}_{new} \leftarrow \{\mathbf{z}_{best}\}$ ▷ Elitism: Preserve global best
  for $k = 1$ to $(N-1)/2$ **do**
    Select parents $\mathbf{p}_1, \mathbf{p}_2 \in \mathbf{Z}$ via tournament selection
    Generate $\mathbf{o}_1, \mathbf{o}_2$ via Sine-Cosine Crossover (SCX) using Eq. 47, 48
    Mutate to $\mathbf{o}_1', \mathbf{o}_2'$ via SCA-Guided Mutation (SCM) using Eq. 49
    $\mathbf{Z}_{new} \leftarrow \mathbf{Z}_{new} \cup \text{clip}(\{\mathbf{o}_1', \mathbf{o}_2'\}, \mathbf{z}_{lb}, \mathbf{z}_{ub})$
  end for
  $\mathbf{Z} \leftarrow \mathbf{Z}_{new}$
  for $\forall \mathbf{z}_i \in \mathbf{Z} \setminus \{\mathbf{z}_{best}\}$ **do** ▷ Evaluate new offspring
    Extract $\mathbf{Q}_{aug}$, $\mathbf{R}$ from $\mathbf{z}_i$; Solve ARE Eq. 36 for $\mathbf{P}$
    $J_i \leftarrow J_{opt}(\mathbf{z}_i)$ via Eq. 42 **if** $\mathbf{P} \succ 0$, **else** $J_i \leftarrow \infty$
    if $J_i < J_{best}$ **then**
      $\mathbf{z}_{best} \leftarrow \mathbf{z}_i$; $J_{best} \leftarrow J_i$
    end if
  end for
end for
return $\mathbf{z}_{best}$

Optimization Results and Statistical Analysis

The optimization framework was implemented for online tuning, utilizing the IGA, GA, PSO, and DE algorithms to directly minimize the IAE fitness function and ascertain the optimal weighting matrices for the ILQR controller. All algorithms were scripted in MATLAB and interfaced with the high-fidelity nonlinear SIMULINK plant model. To ensure a consistent computational budget across all trials, the termination criterion was strictly defined by a maximum iteration count of 100 ($T_{max} = 100$). The simulation horizon for each fitness evaluation was maintained at 10 seconds.

To guarantee a fair and reproducible comparative analysis, all metaheuristic algorithms were configured with identical population sizes and iteration limits. The specific hyperparameters for GA, PSO, DE, and the proposed IGA were calibrated based on empirical tuning and standard literature recommendations for control optimization problems; these details are provided in Table 1.

Upon convergence, each algorithm yielded a unique set of controller parameters. The resulting optimal state feedback gain vector $\mathbf{K_x}$ and integral gain K_i for each method are cataloged in Table 2. Subsequently, the corresponding decision variables—specifically the diagonal elements of the state weighting matrix Q and the scalar control weighting R—are presented in Table 3.

Statistical Analysis

To validate the reliability of the stochastic optimization processes, a statistical analysis of the fitness function and execution time was conducted over 20 independent runs for each algorithm. The statistical metrics for the objective function (IAE) obtained from these trials are summarized in Table 4.

The empirical data unequivocally demonstrates the superiority of the IGA-tuned controller. The proposed method achieved the lowest mean fitness value of **1.9978** and the best optimal cost of **1.97**, outperforming the closest competitor (PSO), which recorded a mean of 2.0163. Furthermore, the standard deviation metric serves as a critical indicator of robustness; the IGA recorded the lowest standard deviation (**0.0117**) and variance (**1.38E-04**). This minimal statistical

Table 1 Configuration of optimization algorithms

Algorithm	Parameter	Value
All	Population Size (N)	30
	Max Iterations (T_{max})	100
GA	Crossover Probability (P_c)	0.95
	Mutation Probability (P_m)	0.02
	Selection Type	Tournament (Size=5)
PSO	Inertia Weight (w)	$0.9 \rightarrow 0.2$
	Accel. Coefficients (c_1, c_2)	1.5, 1.3
DE	Crossover Probability (CR)	0.9
	Scaling Factor (F)	0.8
IGA	SCA Parameter (a)	2.0

Table 2 Optimal ILQR control gains (K) obtained by different algorithms

Algorithm	State Feedback Gain Vector ($\mathbf{K_x}$)	Integral Gain (K_i)
GA	$[430.2090, 189.3873, -419.1805, 16.0672, 85.1953, -19.7287]$	-447.2136
PSO	$[395.9551, 182.6160, -421.8394, 14.0382, 88.9553, -19.9721]$	-387.2983
DE	$[319.2013, 134.3807, -196.6720, 14.8859, 15.8686, -6.1173]$	-316.2278
IGA	$[365.1706, 166.7309, -422.7170, 14.4605, 77.0873, -21.7472]$	-316.2278

Table 3 Optimal ILQR weighting parameters

Algorithm	Matrix Q ($diag([q_1, q_2, \ldots, q_7])$)	Scalar R
IGA	[260, 35, 70, 10, 70, 10, 1000]	0.01
GA	[130, 80, 30, 10, 30, 10, 2000]	0.01
PSO	[130, 80, 30, 10, 30, 10, 1500]	0.01
DE	[150, 65, 70, 1, 70, 1, 1000]	0.01

Table 4 Statistical results of fitness function (IAE) over 20 runs

Algorithm	Mean	Best	Worst	Std. Dev	Variance
GA	2.0233	2.0010	2.0491	0.0125	1.56E-04
PSO	2.0163	1.9900	2.0582	0.0238	5.66E-04
DE	2.0168	1.9802	2.0614	0.0250	6.26E-04
IGA	**1.9978**	**1.9700**	**2.0141**	**0.0117**	**1.38E-04**

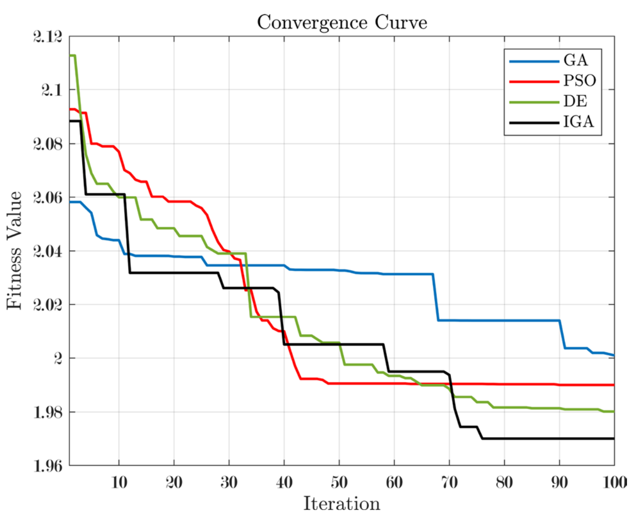

Fig. 3 Convergence curve of the optimization algorithms over 100 iterations

dispersion confirms the algorithm's capability to consistently converge towards the global optimum, irrespective of the initial population distribution. In contrast, the higher variance observed in DE (6.26E-04) and PSO (5.66E-04) suggests a susceptibility to local optima entrapment.

The convergence behavior, illustrated in Fig. 3, further elucidates the search dynamics. The IGA (black line) exhibits a distinct trajectory characterized by a steep initial descent, indicating strong exploration capabilities in the early iterations. Unlike the GA (blue line) and PSO (red line), which exhibit signs of stagnation early in the search process, the IGA maintains a steady improvement, effectively navigating the search space to locate a superior solution around the 75th iteration before plateauing.

Table 5 Statistical comparison of algorithm execution times (hours)

Algorithm	Mean	Best	Worst
GA	2.4843	2.2208	2.8064
PSO	1.7685	1.5844	2.0684
DE	1.8652	1.5700	2.0838
IGA	**1.9843**	**1.6069**	**2.2938**

In terms of computational overhead, Table 5 details the execution time required by each algorithm. While the IGA does not record the absolute lowest mean execution time (1.9843 hours) compared to PSO (1.7685 hours), its trade-off between computational cost and solution quality is favorable. The slight increase in processing time relative to PSO is justified by the significant improvement in solution accuracy and robustness. Moreover, the IGA remains computationally more efficient than the standard GA, which required an average of 2.4843 hours. This balance is attributed to the deterministic SCA operators, which streamline the search process by reducing the reliance on purely stochastic mutation operations.

ANOVA Test

To statistically substantiate the superiority of the proposed method, a One-Way Analysis of Variance (ANOVA) test was employed. This parametric test determines whether the observed differences in the mean IAE values between the IGA and the benchmark algorithms (GA, PSO, DE) are statistically significant or merely the result of random variation. The Null Hypothesis (H_0) posits that the population means of the fitness values for all algorithm groups are equal ($\mu_{IGA} = \mu_{GA} = \mu_{PSO} = \mu_{DE}$). Conversely, the Alternative Hypothesis (H_1) suggests that at least one group mean is significantly different.

The ANOVA procedure decomposes the total variance observed in the dataset into two components: the variance between the algorithm groups (explained variance) and the variance within the groups (unexplained or error variance). The F-statistic is then calculated as the ratio of the Mean Square between groups (MS_{Groups}) to the Mean Square error (MS_{Error}). A larger F-statistic indicates that the variation between the algorithm means dominates the variation within the runs, providing stronger evidence against H_0.

The results of the analysis are detailed in Table 6. The calculated F-statistic of 6.49 indicates a substantial variance between the algorithm performances relative to the internal error variance. Consequently, the obtained P-value is **0.000573**. Since this value is strictly less than the standard significance level of $\alpha = 0.05$ (and indeed $\alpha = 0.001$), the Null Hypothesis is rejected with high confidence. This result provides robust statistical confirmation that the performance improvement achieved by the IGA-tuned ILQR controller is statistically significant and distinct from the results produced by the benchmark algorithms.

The statistical findings are visually corroborated by the boxplot distribution in Fig. 4. The IGA (far left) exhibits a distinctly lower median fitness value compared to GA, PSO, and DE, positioning the entire interquartile range of the proposed method below the medians of the benchmark algorithms. Furthermore, the compact nature of the IGA box indicates a higher degree of consistency and repeatability in locating the optimal solution, whereas the broader distributions observed for PSO and DE reflect a greater susceptibility to stochastic variation and local optima.

An Improved Genetic Algorithm (IGA) mapped the high-dimensional tuning space to locate the global physical limits of the crane system. To maintain strict focus on the physical vibration control problem, the algorithmic mechanics of this optimizer—including Sine Cosine operators and deployment pseudo code. Statistical convergence analysis confirmed that this search architecture yielded the lowest variance among the benchmark methods. This minimal dispersion guarantees the identified physical tuning parameters represent a reliable, algorithm-independent global optimum rather than a localized mathematical artifact.

Table 6 ANOVA results on IAE fitness function

Source	SS	df	MS	F	P-Value
Columns	0.007232	3	0.002411	6.49	**0.000573**
Error	0.028233	76	0.000371		
Total	0.035465	79			

SS: Sum of Squares, df: Degrees of Freedom, MS: Mean Square

F: F-statistic ratio, P-Value: Probability value

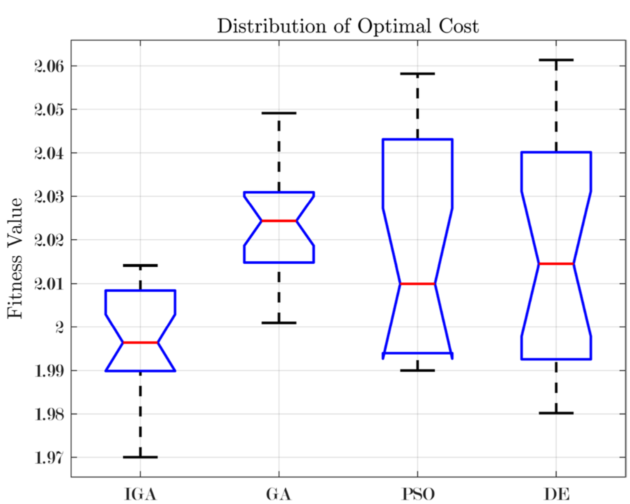

Fig. 4 Boxplot analysis showing the distribution of optimal costs across independent runs

Simulation Results Analysis

To validate the efficacy and robustness of the proposed IGA-ILQR control strategy, a series of comprehensive simulations were conducted. The optimization process, detailed in Section "Improved GA Based ILQR Controller Optimization", was executed using MATLAB 2025a on a computer equipped with an Intel Core i5 processor and 20 GB of RAM. The gantry crane system itself was constructed in the SIMULINK environment, faithfully representing the complete nonlinear dynamic model derived in Section "System Modeling and Preliminaries". All subsequent performance evaluations were carried out by interfacing the optimized controller with this high-fidelity nonlinear plant, ensuring a realistic assessment of the control law's effectiveness.

The physical parameters used for the gantry crane model are defined in Table 7. For the nominal performance test (Section "Dynamical Performance"), the cable length l_1 is set to 0.30 m and the payload mass m_2 is 0.10 Kg. The other specified parameter ranges are utilized in the robustness analysis (Section "Parametric Disturbance Response").

Dynamical Performance

This initial simulation evaluates the dynamical step response ($x_{ref} = 0.4$ m) of the proposed IGA ILQR under nominal parameters, benchmarked against ILQR controllers identically optimized by standard GA, PSO, and DE.

Analysis of the trolley's performance in Fig. 5 confirms the IGA's superiority. It is the only method to achieve a

Table 7 Parameters of the Gantry Crane Model [23]

Variables	Symbol	Values
Trolley Mass	M	1.155 Kg
Hook Mass	m_1	0.20 Kg
Payload Mass	m_2	0.10 Kg
Fixed Cable Length and Varying Cable Length	l_1	0.30 m and 0.20 – 0.40 m
Sling Cable	l_2	0.20 m
Viscous Damping Coefficient of Trolley	f_x	82 Ns/m
Viscous Damping Coefficient of Hoisting	f_l	75 Ns/m
Gravitational Constant	g	9.81 m/s^2

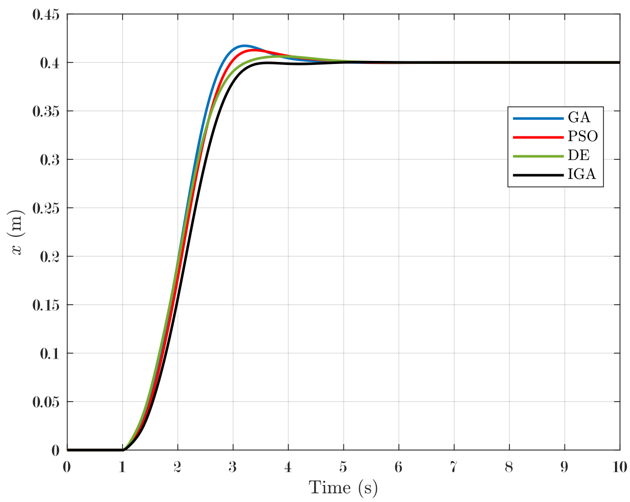

Fig. 5 Trolley response curve: nominal system parameters

critically damped response, eliminating overshoot entirely (0.00%). This contrasts with the overshooting of all benchmarks: 4.30% (GA), 3.19% (PSO), and 1.57% (DE). This optimal transient behavior allows the IGA ILQR to secure the fastest settling time of 2.23 s, substantially quicker than the GA (3.14 s) and PSO (3.3 s).

Crucially, the IGA achieves this superior tracking while simultaneously providing the most effective sway suppression (Figs. 6 and 7), finding a better optimum for the conflicting objectives. The IGA-ILQR minimizes oscillations, limiting the maximum hook sway to 3.2° and the critical payload sway to 4.16°. This is markedly better than all competitors, which induced larger sways, including a payload sway of 5.87° (GA) and 5.84° (DE).

Finally, Fig. 8 reveals a significant practical advantage in the control effort. The IGA-tuned controller generates a notably smoother control signal, avoiding the aggressive peaks of the GA and PSO. This profile implies a more efficient actuator-friendly control action that reduces mechanical stress and energy consumption. A comprehensive quantitative comparison of these performance metrics against the benchmark metaheuristics is provided in Table 8.

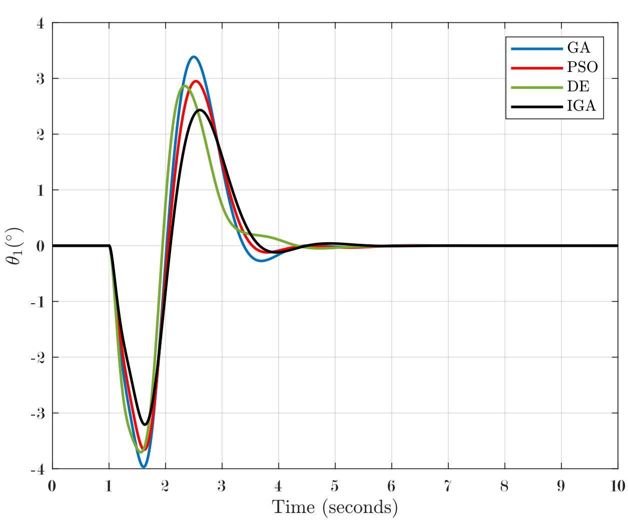

Fig. 6 Hook sway angle: nominal system parameters

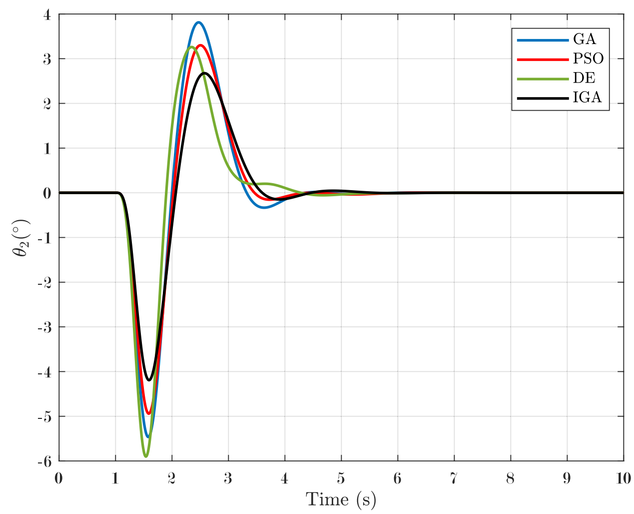

Fig. 7 Payload sway angle: nominal system parameters

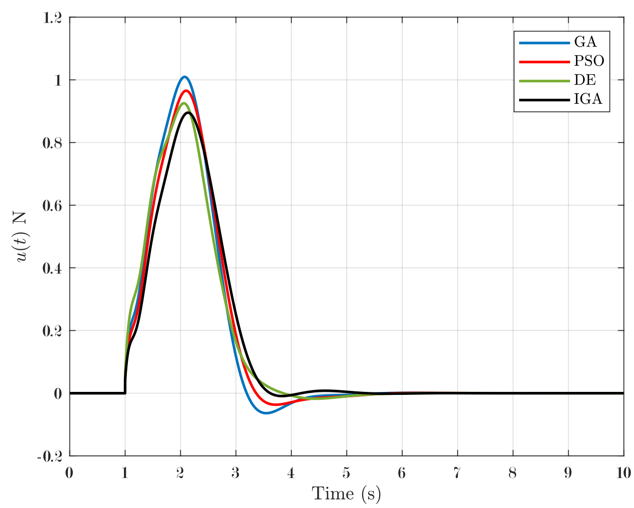

Fig. 8 Control signal curve

Table 8 Comparative assessment of nominal step response performance

Controller	OS%	Settling Time	Rise Time	Max Sway (hook)	Max Sway (payload)
IGA	**0.00%**	**2.23 s**	**1.8 s**	**3.2°**	**4.16°**
GA	4.30%	3.14 s	1.65 s	4°	5.87°
PSO	3.19%	3.3 s	1.65 s	3.91°	4.93°
DE	1.57%	4 s	1.65 s	3.7°	5.84°

Parametric Disturbance Response

While the preceding analysis in Section "Dynamical Performance" established the superior performance of the IGA-ILQR controller under ideal nominal conditions, a controller's practical utility is fundamentally determined by its **robustness**. Real-world industrial environments, such as port logistics, rarely operate with fixed parameters. Gantry cranes must routinely handle payloads of varying mass (m_2), and other physical parameters like cable length (l_1) can differ, leading to significant **parametric uncertainty**. Furthermore, the controller must respond reliably to different operational commands, such as changes in the target destination (x_d). This section, therefore, conducts a comprehensive robustness analysis to evaluate the performance of all four optimized controllers when subjected to these practical variations. The objective is to demonstrate that the proposed IGA-tuned controller not only performs optimally under nominal conditions but also maintains its superior transient response and effective sway suppression.

Scenario 1: Change in Desired Position

This first robustness test evaluates the controller's response to a change in operational command, increasing the target position to $x_d = 0.6$ m. The IGA ILQR controller's robustness is immediately evident in Fig. 9; it maintains its superior, non-overshooting transient response. In contrast, the benchmark controllers' performance degrades, with GA, PSO, and DE all exhibiting noticeable overshoot.

While the more aggressive maneuver understandably increases sway across all systems, Figs. 10 and 11 confirm the IGA's robust sway suppression. The IGA-tuned controller limits the critical payload sway to 6.3°. This is significantly more effective than the benchmarks, which produced larger, more dangerous oscillations, peaking at 8.81° (DE) and 8.2° (GA). The IGA also achieves the minimum hook sway (4.32°).

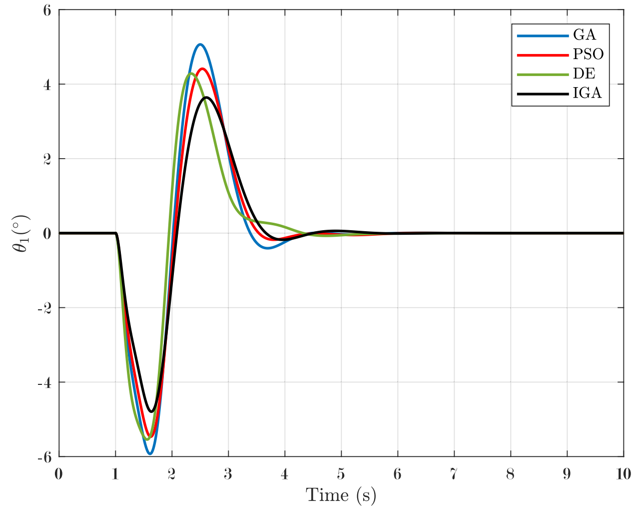

Fig. 10 Hook sway angle when: $x_d = 0.6$ m

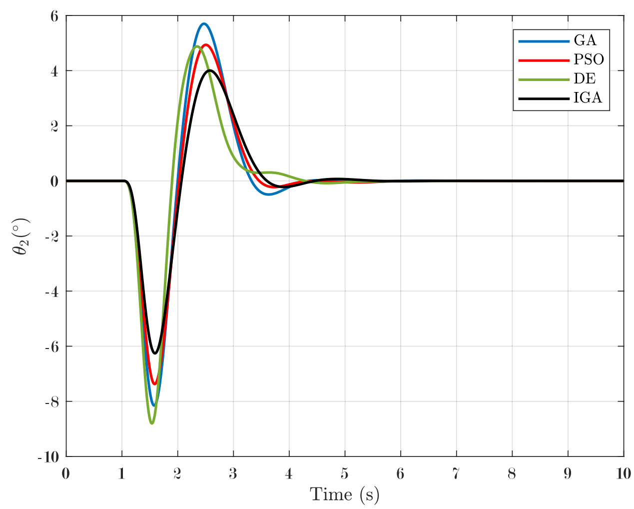

Fig. 11 Payload sway angle when: $x_d = 0.6$ m

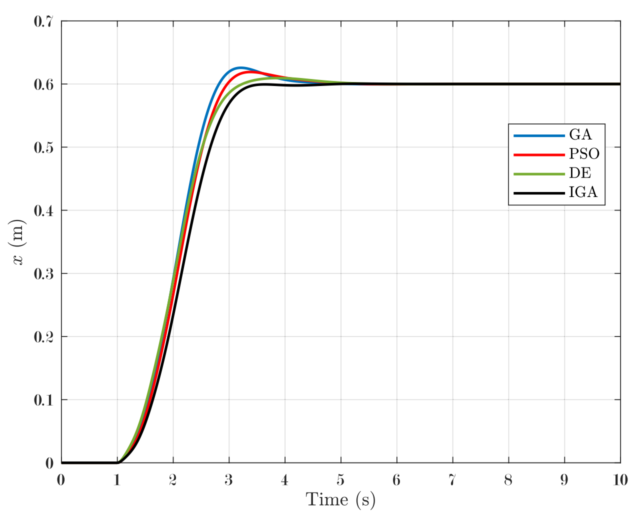

Fig. 9 Trolley response curve when: $x_d = 0.6$ m

Scenario 2: Variation in Payload Mass

This scenario evaluates robustness against parametric uncertainty in the payload mass (m_2), a common occurrence in practical operations. The test was conducted with both a lighter payload ($m_2 = 0.3$ Kg) and a heavier payload ($m_2 = 0.5$ Kg).

The results in Figs. 12 and 13 demonstrate the IGA's superior robustness. It is the only controller to maintain its smooth, non-overshooting tracking response across both mass variations. In contrast, the GA, PSO, and DE

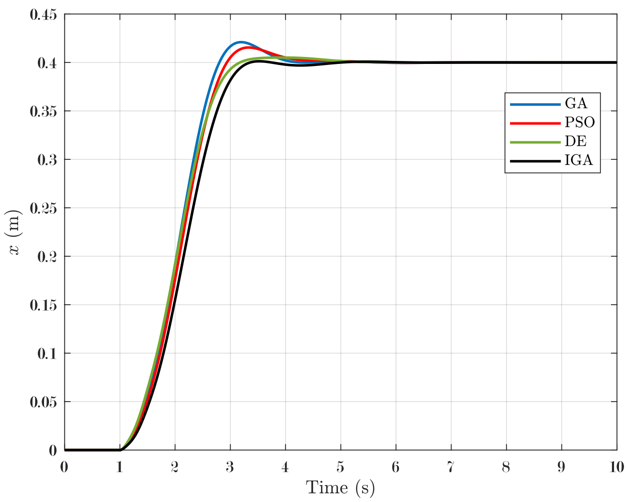

Fig. 12 Trolley response curve when: $m_2 = 0.3$ Kg

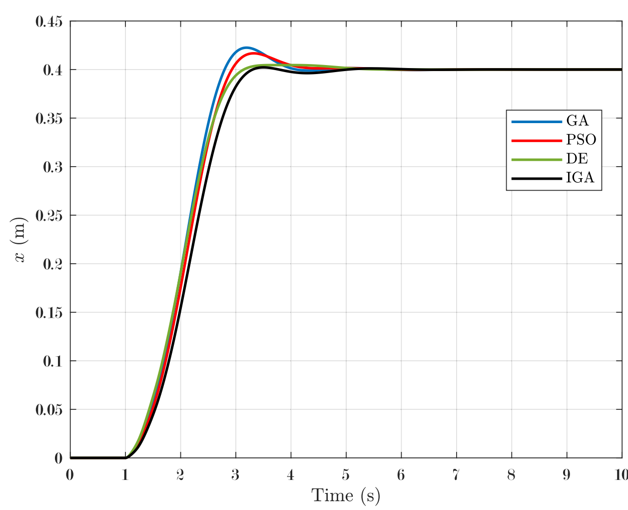

Fig. 13 Trolley response curve when: $m_2 = 0.5$ Kg

controllers all exhibit overshoot, proving their tuning is less robust.

The IGA's lead in sway suppression is maintained, as shown in Figs. 14, 15, 16, and 17. With the lighter 0.3 Kg mass (Figs. 14 and 15), the IGA-ILQR limits the maximum payload sway to 3.48°, outperforming the GA (4.5°) and PSO (4.86°). When tested with the heavier 0.5 Kg mass (Figs. 16 and 17), the IGA again achieves the minimum payload sway at 3.3°, a marked improvement over the GA (4.22°) and DE (4.25°). This consistent performance confirms the IGA identified a highly robust tuning solution.

Scenario 3: Simultaneous Parameter Variations

This final test subjects the controllers to the most challenging conditions: simultaneous variations in cable length

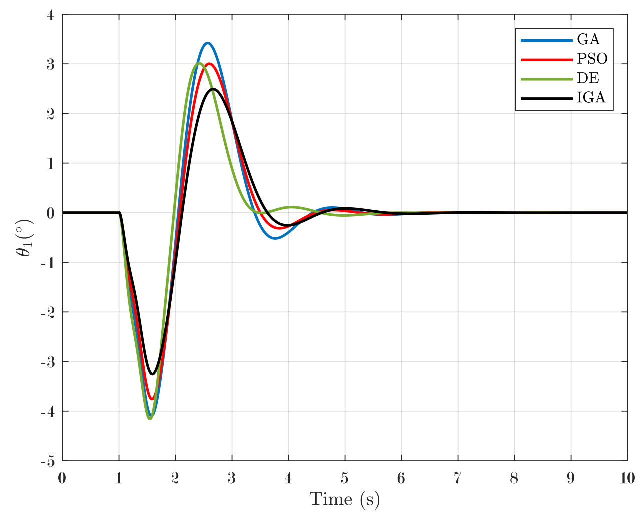

Fig. 14 Hook sway angle when: $m_2 = 0.3$ Kg

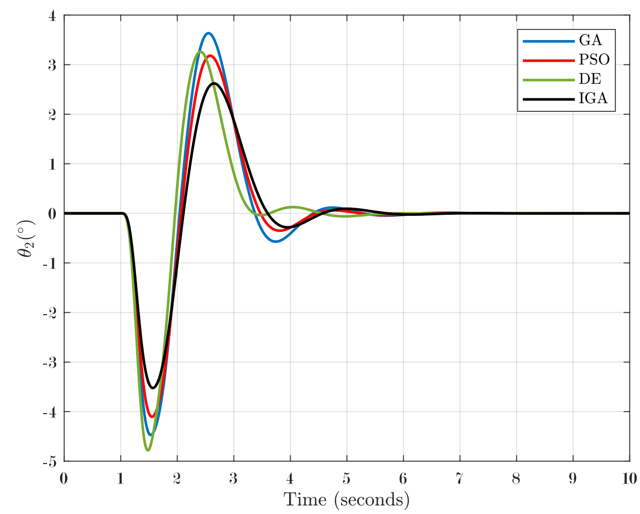

Fig. 15 Payload sway angle when: $m_2 = 0.3$ Kg

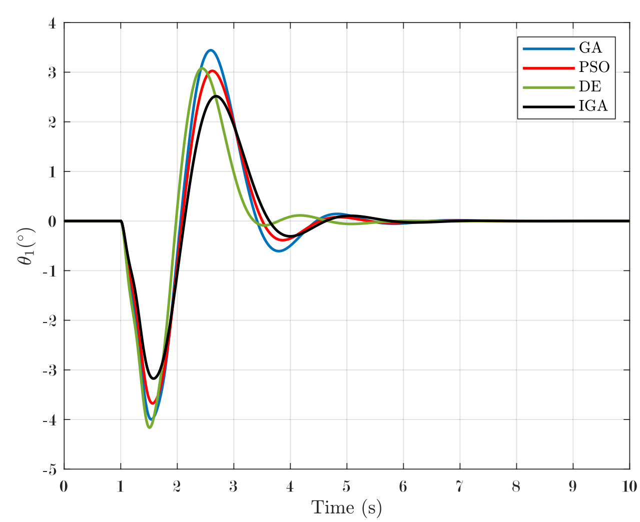

Fig. 16 Hook sway angle when: $m_2 = 0.5$ Kg

($l_1 = 0.4$ m) and payload mass ($m_2 = 0.3$ Kg and $m_2 = 0.5$ Kg). The IGA-ILQR proves its superior robustness, as it is the only controller to maintain a stable, non-overshooting trolley response in both compound test cases (Figs. 18 and 21). The benchmark algorithms, particularly DE, (Fig. 19) exhibit degraded, oscillatory tracking. This trend is confirmed by the sway suppression data (Figs. 20 and 23). The IGA consistently achieves the lowest payload sway, limiting it to ($3.33°$ with $m_2 = 0.3$ Kg) and ($3.29°$ with $m_2 = 0.5$ Kg). This performance far exceeds (Fig. 21) the benchmarks, which recorded sways as high as $4.66°$ (DE) and $4.27°$ (GA), proving the IGA's tuning is robust to complex, simultaneous uncertainties (Fig. 22).

Table 9 provides a consolidated summary of controller performance under all parametric disturbance scenarios. The data presents a clear and consistent trend: the IGA-tuned controller consistently outperforms all benchmarks across every robustness test. In all scenarios involving changes to target position, payload mass, and simultaneous parameter variations, the IGA-ILQR achieved the minimum peak sway for both the hook and the critical payload. This overwhelming evidence demonstrates that the IGA optimization approach successfully located a truly robust, globally optimal set of tuning parameters that the standard meta-heuristics failed to find (Fig. 23).

A physical robustness envelope explicitly characterizes the stability and resilience of the derived ILQR parameters as in Fig. 24. In addition to evaluating isolated time-domain points, this contour map tracks maximum payload sway across a continuous spectrum of physical uncertainties. The analysis sweeps the payload mass from 0.1 to 1.0 kg and the cable length from 0.2 to 0.8 m.

The resulting robustness envelope confirms the controller successfully isolates the payload from chaotic excitation across all tested boundaries. Maximum payload sway remains strictly bounded below $3.5°$ across the entire evaluated spectrum of mass and cable length variations. The optimized parameters maintain an expansive safety margin well below the critical $10°$ operational limit. Mapping this two-dimensional parameter space secures the physical robustness limits of the double-pendulum dynamics. This provides a highly resilient, quantifiable control methodology for practical industrial implementation.

Discussion

The comprehensive simulation results validate the proposed optimal state-feedback control architecture. The critical finding extends beyond the superior nominal performance detailed in Section "Dynamical Performance" to demonstrate consistent robustness across a broad spectrum of

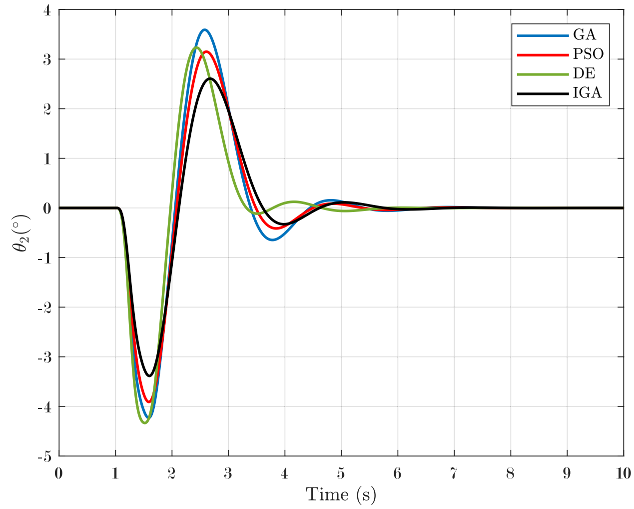

Fig. 17 Payload sway angle when: $m_2 = 0.5$ Kg

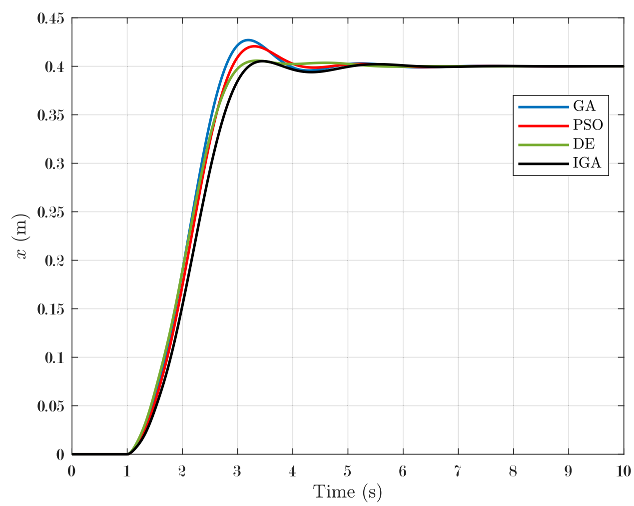

Fig. 18 Trolley response curve when: $m_2 = 0.3$ Kg and $l_1 = 0.4$ m

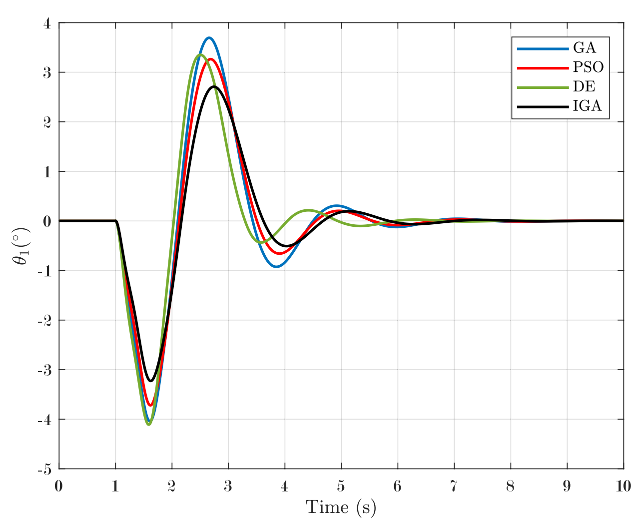

Fig. 19 Hook sway angle when: $m_2 = 0.3$ Kg and $l_1 = 0.4$ m

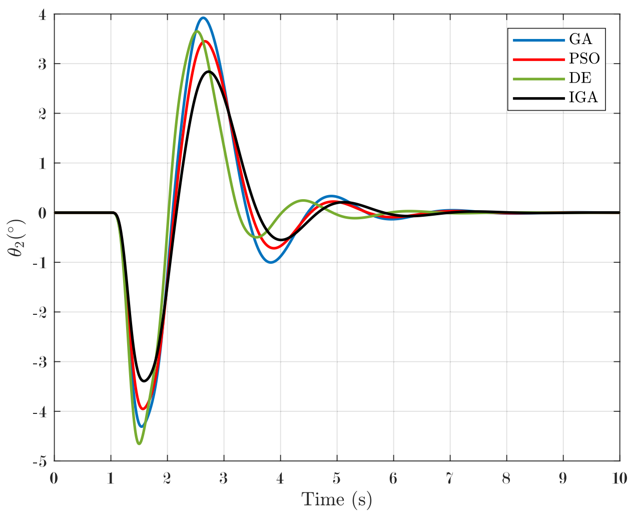

Fig. 20 Payload sway angle when: $m_2 = 0.3$ Kg and $l_1 = 0.4$ m

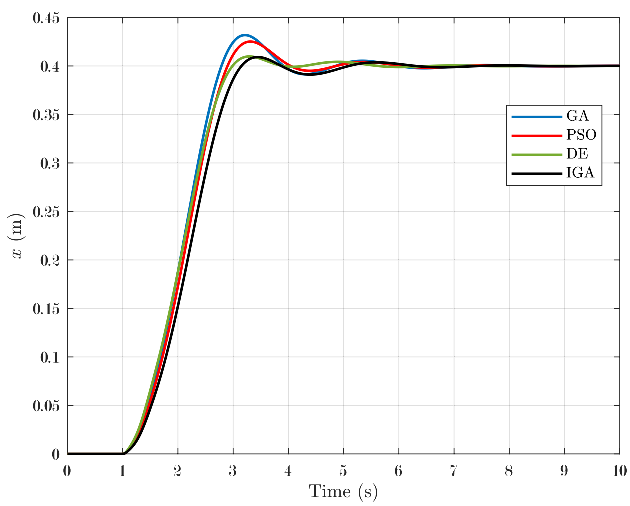

Fig. 21 Trolley response curve when: $m_2 = 0.5$ Kg and $l_1 = 0.4$ m

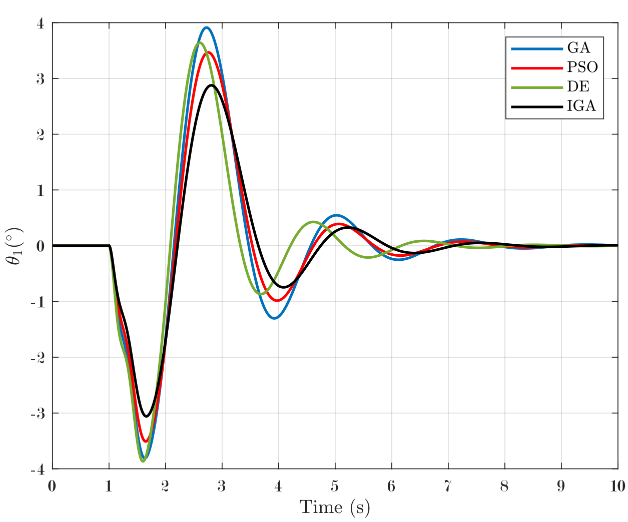

Fig. 22 Hook sway angle when: $m_2 = 0.5$ Kg and $l_1 = 0.4$ m

Table 9 Consolidated sway performance under parametric disturbance scenarios

Scenario	Controller	Max Hook Sway (deg)	Max Payload Sway (deg)
Scenario 1	**IGA**	**4.32**	**6.30**
($x_d = 0.6m$)	GA	5.97	8.20
	PSO	4.80	7.30
	DE	4.82	8.81
Scenario 2	**IGA**	**3.18**	**3.48**
($m_2 = 0.3Kg$)	GA	4.10	4.50
	PSO	3.76	4.86
	DE	4.13	4.12
Scenario 2	**IGA**	**3.14**	**3.30**
($m_2 = 0.5Kg$)	GA	4.00	4.22
	PSO	3.73	3.89
	DE	4.11	4.25
Scenario 3	**IGA**	**3.18**	**3.33**
($l_1, m_2 vary$)	GA	4.02	4.27
	PSO	3.74	3.97
	DE	4.05	4.66
Scenario 3	**IGA**	**3.02**	**3.29**
($l_1, m_2 vary$)	GA	3.86	4.18
	PSO	3.52	3.95
	DE	3.87	4.20

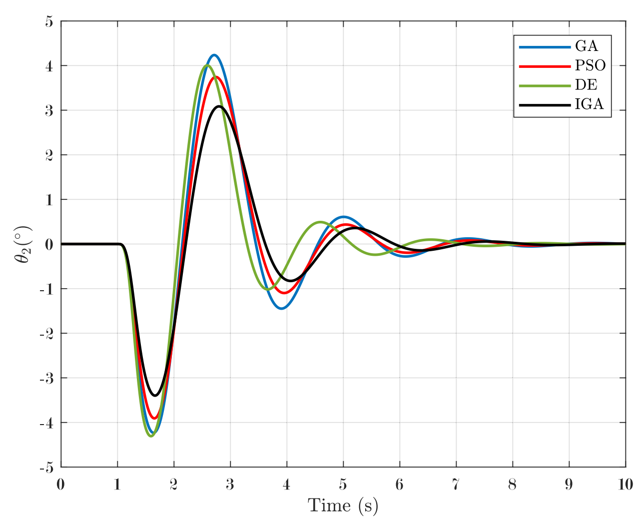

Fig. 23 Payload sway angle when: $m_2 = 0.5$ Kg and $l_1 = 0.4$ m

parametric disturbances evaluated in Section "Parametric Disturbance Response". This directly addresses a primary limitation in classical optimal control: overcoming the brittle nature of heuristically tuned LQR controllers that become over-fitted to a single operating point. By mapping the global physical limits of the system using the optimization framework detailed in Section "Improved GA Based ILQR Controller Optimization", the tuning methodology

Fig. 24 Robustness envelope: ILQR-IGA

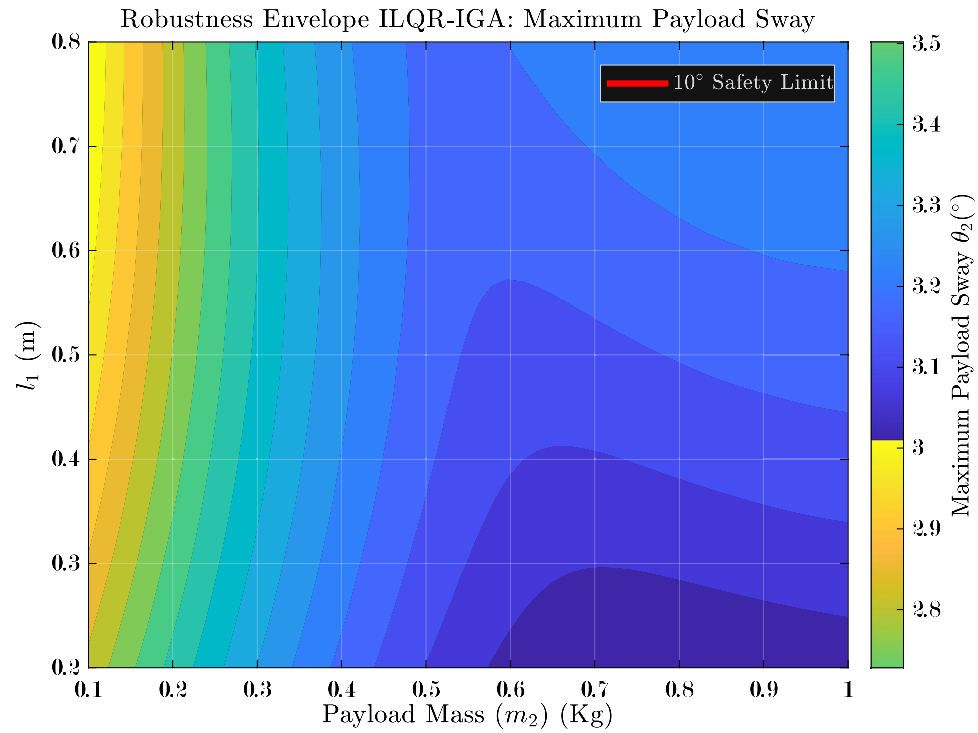

successfully identified a single, fixed-gain controller inherently robust to significant operational and parametric variations without requiring highly complex adaptive or gain-scheduling architectures.

Transferable Sway-Suppression Design Guidance

Extracting transferable ILQR design guidance for double-pendulum gantry cranes forms the core engineering contribution of this study. The optimal weighting matrices (Q_{aug} and R) isolated during the global search reveal a distinct physical strategy for managing underactuated, chaotic dynamics.

1. **The Dynamic Absorber Principle:** Analyzing the optimal state penalties indicates that robust sway suppression demands an asymmetric weighting strategy. The controller penalizes payload sway twice as heavily as hook sway ($Q_{\text{payload}} = 70$ versus $Q_{\text{hook}} = 35$). Within the evaluated parameters, this suggests a practical design guideline: the intermediate hook mass must be permitted a larger sway tolerance to function as a dynamic energy absorber. This controlled oscillation dissipates kinetic energy, effectively insulating the critical payload from transit-induced excitation.
2. **Active Damping at the Source:** Velocity state penalties dictate that active damping must be prioritized at the primary pivot. The optimal robustness envelope heavily penalizes the hook's angular velocity ($Q_{\text{hook\_velocity}} = 70$) while relaxing the constraint on the payload's angular velocity ($Q_{\text{payload\_velocity}} = 10$). The trolley actuator resides kinetically closest to the hook. Aggressively arresting the hook's momentum at this source prevents unmitigated energy from propagating down the kinematic chain to the payload.
3. **Integral Dominance:** The successful tuning strategy relies on an exceptionally high integral penalty ($Q_{\text{integral}} = 1000$) paired with a relaxed control effort penalty ($R = 0.01$). Catching chaotic dynamic shifts quickly and enforcing zero steady-state error under varying masses requires this specific balance. For practical double-pendulum applications, this dictates a strict hardware requirement: actuators must possess the bandwidth to execute rapid, high-frequency force corrections to preserve the stability envelope over extended operational timeframes.

To validate that the observed stability of the crane represents a robust, empirically derived characteristic within the studied operational domain of the control architecture rather than a mathematical artifact of the search process, a comparative robustness envelope was generated using the baseline standard GA as in Fig. 25. As demonstrated, the properly formulated ILQR framework ensures a fundamental safety limit independent of the optimizer; even the baseline GA maintains the maximum

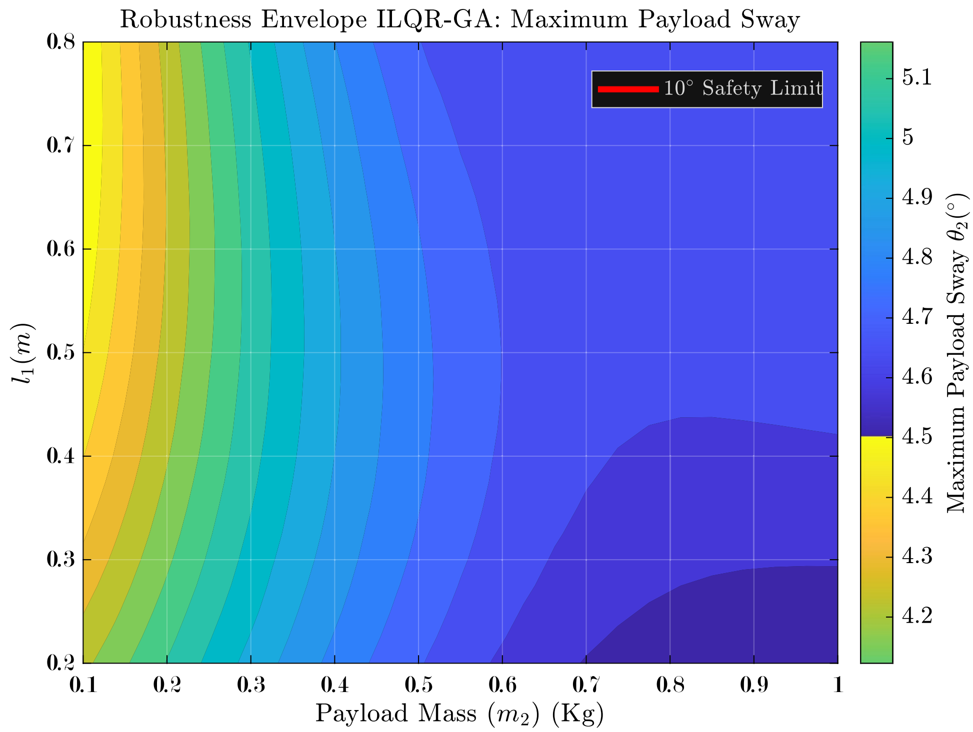

Fig. 25 Robustness envelope: ILQR-GA

movement of the payload well below the critical limit 10° , peaking at 5.1° under worst-case parametric uncertainties (low payload mass and high cable length). However, the IGA's superior adherence to the Dynamic Absorber Principle—optimally balancing the hook and payload penalties where the GA failed—allows it to significantly compress this physical envelope, limiting worst-case sway to just 3.5°. This comparative analysis proves to control engineers that while the baseline stability envelope is a physical property of the ILQR design, utilizing advanced optimization tools provides a distinctly superior margin of industrial safety.

It is imperative to explicitly define the scope of applicability for these design insights. The derived robustness envelopes and sway-suppression trends are intrinsically linked to the modeling assumptions of this specific double-pendulum gantry crane, notably the linearization of the dynamics around the equilibrium point and the structural formulation of the ILQR. Furthermore, the numerical boundaries of the stability envelope apply directly to the evaluated parameter ranges (e.g., payload mass variations from 0.1 to 1.0 kg and cable lengths from 0.2 to 0.8 m). While the optimization framework served as a highly effective supporting tool to uncover these optimal weightings, extrapolating these specific numerical values to distinctly different crane configurations (e.g., tower cranes or systems with simultaneous hoisting maneuvers) would require re-evaluating the system's unique kinematic constraints.

Practical Industrial Implications

Beyond strict vibration attenuation, the derived robustness envelope yields significant practical advantages for industrial implementation. The optimized controller generates a distinctly smoother, less aggressive control signal (Fig. 8) compared to standard heuristic tuning. This profile directly implies reduced mechanical stress on trolley actuators and lower overall energy consumption. The ability to systematically identify an operating envelope that naturally balances high-precision payload positioning with actuator-friendly control action ensures the system's longevity and viability in continuous-duty maritime and manufacturing environments.

Conclusions

This paper addressed the formidable challenge of tuning an Integral LQR controller for the underactuated, nonlinear dynamics of a double-pendulum gantry crane. By hybridizing the Genetic Algorithm with deterministic Sine Cosine operators, we developed a novel Improved Genetic Algorithm (IGA) engineered to escape the local optima that entrap standard metaheuristics.

A comparative study against GA, PSO, and DE-tuned controllers confirmed the superior efficacy of the proposed method. The findings are substantiated by three key performance indicators:

- **Statistical Significance:** The reliability of these improvements was validated through statistical analysis over 20 independent runs. The IGA exhibited the lowest standard deviation (0.0117), indicating superior convergence consistency. Furthermore, a one-way ANOVA test yielded a P-value of 5.73×10^{-4}, confirming with high confidence ($P < 0.001$) that the performance gains are statistically significant and distinct from random algorithmic variations.
- **Dynamical Superiority:** The IGA-ILQR was the unique solution to achieve a critically damped response with zero trolley overshoot (0%), contrasting with up to 4.30% in benchmarks. Simultaneously, it secured the fastest settling time (2.23 s) and reduced nominal payload sway to $4.16°$, a 29.1% improvement over the standard GA.
- **Robustness under Uncertainty:** Superior performance extended beyond nominal conditions. In scenarios involving simultaneous variations in cable length and payload mass, the IGA-tuned controller maintained strict sway suppression—limiting payload oscillations to just $3.29°$—where benchmark controllers degraded significantly.

Ultimately, this work demonstrates that balancing exploration and exploitation via deterministic operators allows the IGA to locate a more globally optimal region within the 8-dimensional tuning space. The resulting control law not only guarantees robust anti-sway performance but also yields a smoother, actuator-friendly control signal, establishing a practical framework for high-precision industrial crane automation.

Supplementary information

Not available.

Acknowledgements Not available..

Funding Open access funding provided by The Ministry of Higher Education Malaysia and Universiti Teknologi Malaysia

Declarations

Competing Interests The authors declare that they have no known competing financial interests or personal relationships that could have appeared to influence the work reported in this paper.

References

1. Hong K-S, Shah UH (2019) Dynamics and Control of Industrial Cranes. Springer, Singapore
2. Ramli L, Mohamed Z, Abdullahi AM, Jaafar HI, Lazim IM (2017) Control strategies for crane systems: A comprehensive review. Mech Syst Signal Process 95:1–23
3. Hyla P (2012) The crane control systems: A survey. In: 2012 17th International conference on Methods & Models in Automation & Robotics (MMAR), pp 505–509. IEEE
4. Mojallizadeh MR, Brogliato B, Prieur C (2023) Modeling and control of overhead cranes: A tutorial overview and perspectives. Annu Rev Control 56:100877
5. Qian D, Yi J (2016) Hierarchical sliding mode control for underactuated cranes. Springer, Heidelberg, Ber
6. Maghsoudi MJ, Mohamed Z, Husain AR, Tokhi MO (2016) An optimal performance control scheme for a 3d crane. Mech Syst Signal Process 66:756–768
7. Elhabib MO, Wahid H, Mohamed Z, Shutari H (2024) Adaptive genetic algorithm based lqr for optimal control of nonlinear double pendulum gantry crane. In: International symposium on systems modelling and simulation, pp 322–337. Springer
8. Önen Ü, Cakan A, Ilhan I (2019) Performance comparison of optimization algorithms in lqr controller design for a nonlinear system. Turk J Electr Eng Comput Sci 27(3):1938–1953
9. Eltayeb A, Ahmed G, Imran IH, Alyazidi NM, Abubaker A (2024) Comparative analysis: Fractional pid vs. pid controllers for robotic arm using genetic algorithm optimization. Automation 5(3):230–245
10. Jaafar H, Mohamed Z, Mohd Subha N, Husain A, Ismail F, Ramli L, Tokhi M, Shamsudin M (2019) Efficient control of a nonlinear double-pendulum overhead crane with sensorless payload motion using an improved pso-tuned pid controller. J Vib Control 25(4):907–921
11. Katoch S, Chauhan SS, Kumar V (2021) A review on genetic algorithm: past, present, and future. Multimed Tools Appl 80(5):8091–8126
12. Wang Z, Sobey A (2020) A comparative review between genetic algorithm use in composite optimisation and the state-of-the-art in evolutionary computation. Compos Struct 233:111739
13. Joseph SB, Dada EG, Abidemi A, Oyewola DO, Khammas BM (2022) Metaheuristic algorithms for pid controller parameters tuning: Review, approaches and open problems. Heliyon 8(5)
14. Abualigah L, Dulaimi AJ (2021) A novel feature selection method for data mining tasks using hybrid sine cosine algorithm and genetic algorithm. Clust Comput 24(3):2161–2176
15. Rizk-Allah RM, Hassanien AE (2023) A comprehensive survey on the sine-cosine optimization algorithm. Artif Intell Rev 56(6):4801–4858
16. Zhang J, Chung HS-H, Lo W-L (2007) Clustering-based adaptive crossover and mutation probabilities for genetic algorithms. IEEE Trans Evol Comput 11(3):326–335
17. Li Y-B, Sang H-B, Xiong X, Li Y-R (2021) An improved adaptive genetic algorithm for two-dimensional rectangular packing problem. Appl Sci 11(1):413

18. Jakobović D, Golub M (1999) Adaptive genetic algorithm. J Comput Inf Technol 7(3):229–235
19. Karami AH, Hasanzadeh M (2015) An adaptive genetic algorithm for robot motion planning in 2d complex environments. Comput Electric Eng 43:317–329
20. Ye F, Chen J, Tian Y, Jiang T (2020) Cooperative task assignment of a heterogeneous multi-uav system using an adaptive genetic algorithm. Electronics 9(4):687
21. Habib M, Khoucha F, Harrag A (2017) Ga-based robust lqr controller for interleaved boost dc-dc converter improving fuel cell voltage regulation. Electric Power Syst Res 152:438–456
22. Zhao W, Gu L (2023) Hybrid particle swarm optimization genetic lqr controller for active suspension. Appl Sci 13(14):8204
23. Hussien SYS, Jaafar HI, Ghazali R, Ghazaly MM, Johari MKA, Ramli L (2024) Modelling, simulation and validation for a multimode double-pendulum overhead crane. Applic Model Simul 8:261–271
24. Lewis FL, Vrabie D, Syrmos VL (2012) Optimal Control. John Wiley & Sons, ???
25. Naidu DS (2018) Optimal control systems. CRC Press, Boca Raton
26. Mirjalili S (2016) Sca: a sine cosine algorithm for solving optimization problems. Knowl-Based Syst 96:120–133